Journal of Photochemistry and Photobiology A: Chemistry 343 (2017) 7–16

Contents lists available at ScienceDirect

Journal of Photochemistry and Photobiology A: Chemistry

journal homepage: www.elsevier.com/locate/jphotochem

A reactive primary fluorescence switch-on sensor for Hg^{2+} and the generated fluorophore as secondary recognition receptor toward Cu^{2+} in aqueous acetonitrile solution

Srimanta Manna[a], Parthasarathi Karmakar[a], Kalipada Maiti[a], Syed Samim Ali[a], Debasish Mandal[b], Ajit Kumar Mahapatra[a,*]

[a] Department of Chemistry, Indian Institute of Engineering Science and Technology, Shibpur, Howrah, 711103, West Bengal, India
[b] Institute of Chemistry, The Hebrew University of Jerusalem, 91904, Jerusalem, Israel

ARTICLE INFO

Article history:
Received 5 January 2017
Received in revised form 31 March 2017
Accepted 10 April 2017
Available online 13 April 2017

Keywords:
Relay recognition
Metal ion→metal ion sequence
Combination of the chemodosimeter and chemosensor
Mercury and copper
Living cells

ABSTRACT

A new N-methylbenzoimidazole-based fluorescence "turn-on" chemodosimeter (**VPBA**) was synthesized and characterized for cation to cation relay recognition (CCRR) with high sequence specificity ($Hg^{2+} \rightarrow Cu^{2+}$). The selectivity and sensitivity of **VPBA** have been explored in aqueous acetonitrile solution through a specific cyclization reaction triggered by the mercury-promoted hydrolysis of the vinylether group with a significant change of fluorescence color. The probe displayed a fast switch-on fluorescence response with 164 fold toward Hg^{2+}in aquoues acetonitrile solution. Further, the in situ system generated from the sensing of Hg^{2+} showed good relay recognition ability for Cu^{2+} via fast fluorescence quenching by the formation of a 1:2 complex in aquoues acetonitrile. The complexation of Cu^{2+} by **VPBA** has been addressed by HR-MS, ^{1}H NMR, and UV−vis spectra. The probe and their Cu-complex structures have been established by DFT calculations. TDDFT calculations were also performed in order to demonstrate the electronic properties of probe and their copper complex. By using the new strategy, the novel probe could be used for the detection of Hg^{2+} in real-life water samples with good recovery. The probe could be successfully used for the fluorescence image of Hg^{2+} in living cells. These results suggested that the probe has promising applications for Hg^{2+} sensing in biological and environmental sciences.

1. Introduction

There is great interest in the development of good bifunctional chemosensors for the detection of heavy metal ions sequentially based on a single host that can independently recognize two guest species with distinct spectra responses [1]. Recently, this idea has gradually become a new research focus in the field of colorimetric and fluorescent chemosensors [2–9]. Compared to one-to-one analysis methods, detection methods for numerous metal ions with differential responses have advantages of being more efficient and less expensive. Zhou et al. proposed, an excellent dual chemosensor that can detect Cu^{2+} and Hg^{2+} by monitoring changes in UV absorption and the fluorescence spectral pattern has been developed [10]. Recently, we have also reported bifunctional probe that include combination of Hg^{2+}/Zn^{2+} [11].

Mercury (Hg^{2+}) is considered as one of the most hazardous environmental pollutant exist as elemental, inorganic, and organic mercury forms [12,13]. It is widely distributed in air, water, and soil through different processes such as volcanic emissions, mining, solid waste incineration, and the combustion of fossil fuels [14–18]. It is a considerably dangerous metal to human life and ecology even at low concentrations. Among the serious health consequences due to the presence of Hg^{2+} in the human body are prenatal brain damage, DNA damage, various cognitive and motion disorders, Minamata disease, myocardial infarction, some kinds of autism and damage of the brain, kidneys, central nervous system, immune system and endocrine system [19–23]. On the other hand, copper (Cu^{2+}) is an essential trace element in humans, and is found at low levels in a variety of cells and tissues with the highest concentrations in the liver, and in the brain [24]. However, the deficiency and the excess of Cu^{2+} lead to anemia, gastrointestinal, Wilson disease and neurodegenerative syndromes [25–27]. Therefore, the development of a new approach with high sensitivity and specificity toward Hg^{2+} and Cu^{2+} is highly desirable

* Corresponding author.
E-mail address: mahapatra574@gmail.com (A.K. Mahapatra).

http://dx.doi.org/10.1016/j.jphotochem.2017.04.011
1010-6030/

as these two ions are spectroscopically and magnetically silent Hg^{2+} and a paramagnetic Cu^{2+} deserves special attention by scientists across different disciplines.

In the past several years, considerable efforts have been made to develop chemosensors for the detection of Hg^{2+} and Cu^{2+}, especially, for Hg^{2+} based on the coordination to heteroatom, Hg^{2+} catalyzed desulfurization, and Hg^{2+} promoted hydrolysis of the vinylether group and β-alkynyl ether group [28–36]. However, most of them still have some limitations as Hg^{2+} ions are known to produce fluorescence quenching when binding to fluoroionophore molecules via the spin–orbit coupling effect (closed-shell d10 configuration) as well as interference from other coexisting metal ions and poor water-solubility problem [37–40]. Therefore, for practical applications, it is still desirable to develop simple Hg^{2+} sensors with turn-on response, good water solubility and high selectivity and sensitivity. In this context, we propose sequential cation to cation relay recognition (CCRR) of Hg^{2+} and Cu^{2+} based on the specific chemical reaction (chemodosimeter) and followed by chemosensor approaches [41,42].

Our research group is actively engaged in the development of novel selective and sensitive fluorescent chemodosimetric probes for toxic ions [43–47]. Therefore, the present paper deals with the reaction-based fluorescent sensing approach for inorganic mercury species (Hg^{2+}) via Hg^{2+} ion-promoted hydrolysis of vinylether to form the corresponding hydroxyl group. We proposed that the Hg^{2+} ion promoted hydrolysis of the vinyl enol ether group in probe VPBA would generate the hydroxy intermediate, which will readily spontaneous cyclize to form iminocoumarin−N-methylbenzoimidazole that demonstrates significant improvement of fluorescence performance of the probe. As in situ generation of iminocoumarin after Hg^{2+} reaction and it has several binding sites exist for coordination, so it would be expected to serve as a relay probe for the sensing of Cu^{2+} metal ion, by eliciting differences in their absorption and emission spectroscopy.

2. Experimental

2.1. Apparatus and reagents

Unless otherwise mentioned, materials were purchased from Sigma Aldrich and were used without further purification. A Brucker 400 MHz instrument was used to record ^{1}H and ^{13}C NMR spectra. For NMR spectra, $CDCl_3$ and DMSO-d_6 were used as solvent using TMS as an internal standard. Chemical shifts were reported in δ ppm units and ^{1}H–^{1}H and ^{1}H—C coupling constants in Hz. A Waters QTOF Micro YA 263 mass spectrometer was used to record Mass spectra. UV spectra were recorded on a JASCO V-530 spectrophotometer. Fluorescence spectra were obtained using on a Perkin Elmer Model LS 55 spectrophotometer.

2.2. Design and synthetic scheme of probe ***VPBA***

Our underlying principle in the design of a colorimetric and turn-on chemodosimeter probe VPBA was depicted in Scheme 1. The oxymercuration–hydrolysis reaction of the vinyl ether group in VPBA would generate the hydrolyzed product—alkylmercury species $HgCl(CH_2CHO)$ and phenolate ion, which would undergo subsequent intramolecular nucleophilic attack on the α,β-unsaturated nitrile moiety by 1,2-addition and in 6-exo-dig fashion to produce imine anion intermediate. This transient species would quickly abstract a proton from the solvent and eventually lead to the cyclized product iminocoumarin-benzo-

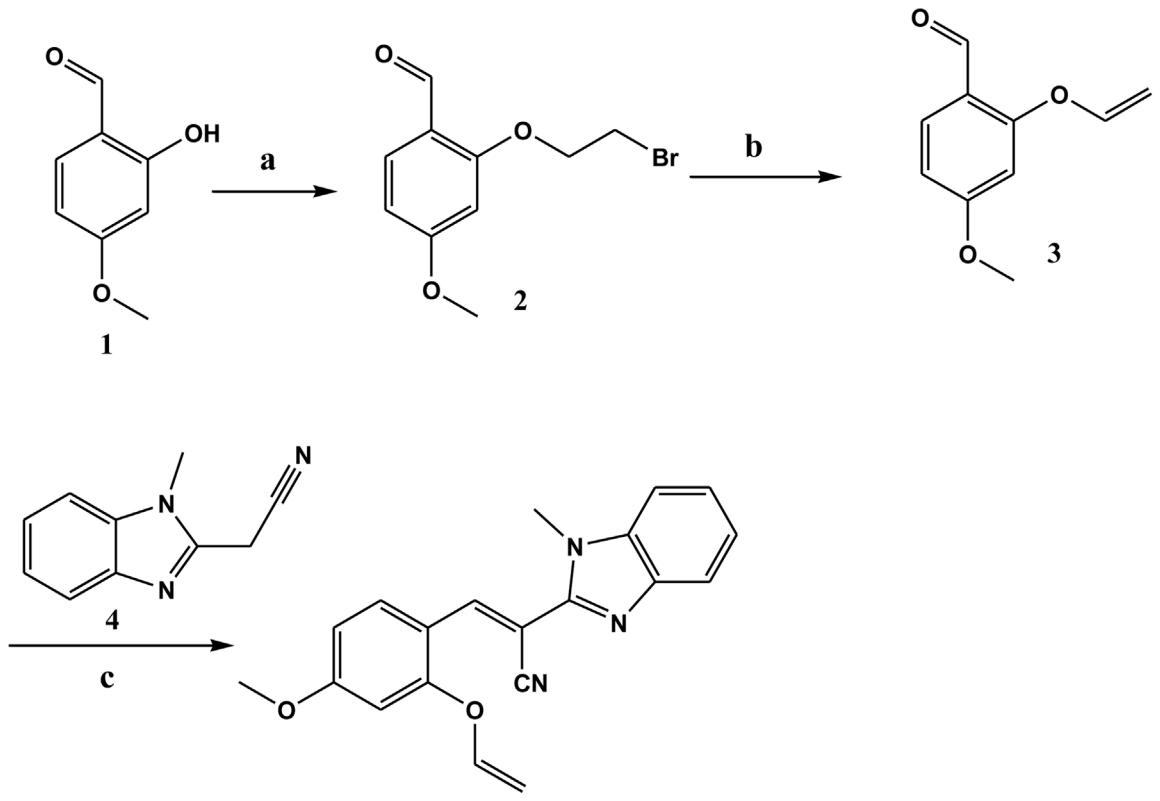

Scheme 1. Synthesis of VPBA.

imidazole **5**, which was responsible for the dramatic fluorescence enhancement. Because vinyl ether **VPBA** was almost non-fluorescent but the product iminocoumarin-benzo-imidazole **5** was highly fluorescent, we could realize a turn-on-type sensing. All the precursors and probe molecules were characterized by various analytical and spectral techniques, such as ^{1}H and ^{13}C NMR and LCMS (Supporting information).

The vinyl ether probe molecule, VPBA, has been synthesized in three steps starting from commercially available 2-hydroxy-4-methoxybenzaldehyde **1** by reacting with 1,2-dibromoethane to form 2-(2-bromoethoxy)-4-methoxybenzaldehyde **2** and subsequent elimination process results in the formation of vinyl ether 3 (Scheme 1). Reagents & Conditions: (a) 1,2-dibromoethane, K_2CO_3, acetone, reflux, 12 h, 35% (b) $KOBu^t$, DMSO, RT, 1 h, 41.6% (c) Piperidine, ethanol, RT, 1 h, 44.8%

2.3. Synthesis of probe *VPBA*

2.3.1. Preparation of 2-(2-Bromo-ethoxy)-4-methoxy-benzaldehyde (*2*)

A mixture of 2-Hydroxy-4-methoxy-benzaldehyde (**1**) (500 mg, 3.28 mmol) in acetone (22 mL) was added K_2CO_3 (453 mg, 3.28 mmol) at RT. To this reaction mixture, 1, 2-dibromoethane (3.2 g, 17.05 mmol) was added. The resulting reaction mixture was heated at 60 °C for 12 h. TLC showed that majority of the starting material was consumed. The reaction mixture was partitioned between ethyl acetate and water. The combined organic solution was washed with brine, dried over sodium sulfate and then concentrated. The crude mixture was purified by column chromatography on silica, product eluted with 5% ethyl acetate in hexane to afford 2-(2-Bromo-ethoxy)-4-methoxy-benzaldehyde (**2**) (300 mg, 35%) as white solid. ^{1}HNMR (400 MHz, $CDCl_3$): δ (ppm) = 10.35 (s, 1H), 7.83 (d, *J* = 8.72 Hz, 1H), 6.59 (d, *J* = 8.4 Hz, 1H), 6.40 (s, 1H), 4.37 (t, *J* = 5.92 Hz, 2H), 3.86 (s, 3H), 3.69 (t, *J* = 5 Hz, 2H). MS (ESI): *m*/*z* calc. for $C_{10}H_{11}Br\,O_3$: 259.10; found: 261.09 $[M+H]^+$.

2.3.2. Preparation of 4-methoxy-2-vinyloxy-benzaldehyde (3)

Under cooling condition, potassium tert butoxide (100 mg, 0.89 mmol) was taken in DMSO (0.3 mL). To this reaction mixture, a solution of 2-(2-Bromo-ethoxy)-4-methoxy-benzaldehyde (**2**) (210 mg, 0.81 mmol) in DMSO (1.4 mL) was added drop wise at 0 °C. The reaction mixture was then stirred at RT for 1 h. TLC showed SM was consumed and the RM was partitioned between ethyl acetate and water. The combined organic solution was washed with brine, dried over sodium sulfate and concentrated. The crude mixture was purified by column chromatography on silica, product eluted with 10% ethyl acetate in hexane to 4-methoxy-2-vinyloxy-benzaldehyde (**3**) (60 mg, 41.6%) as sticky colorless liquid. ^{1}HNMR (400 MHz, $CDCl_3$): δ (ppm) = 10.27 (s, 1H), 7.84 (d, *J* = 8.72 Hz, 1H), 6.69-6.63 (m, 2H), 6.52 (d, *J* = 2.2 Hz, 1H), 4.90-4.86 (m, 1H), 4.62-4.60 (m, 1H), 3.86 (s, 3H). MS (ESI): *m*/*z* calc. for $C_{10}H_{10}O_3$: 178.06; found: 179.0 $[M+H]^+$.

2.3.3. Preparation of (1-Methyl-1H-benzoimidazol-2-yl)-acetonitrile (*4*)

A mixture of N-Methyl-benzene-1,2-diamine (250 mg, 2.04 mmol) and cyanoacetic acid (348 mg, 4.09 mmol) in ethylene glycol (10 mL) was heated at 165 °C for 2 h. TLC showed SM was consumed and formed a desired polar spot with major undesired. The reaction mixture was diluted with ethyl acetate. The organic layer was washed with water followed by the brine washing. The combined organic solution was dried over sodium sulfate and then concentrated. The crude mass was purified by column chromatography on silica, eluted with 1% methanol in DCM to afford (1-Methyl-1*H*-benzoimidazol-2-yl)-acetonitrile (**4**) (50 mg, 14%) as pink solid.

^{1}HNMR (400 MHz, DMSO-d_6): δ (ppm) = 7.62 (d, *J* = 7.72 Hz, 1H), 7.54 (d, *J* = 8.04, 1H), 7.28-7.19 (m, 2H), 4.52 (s, 2H), 3.76 (s, 3H). MS (ESI): *m*/*z* calc. for $C_{10}H_9N_3$: 171.08; found: 172.1$[M+H]^+$.

2.3.4. Preparation of 3-(4-methoxy-2-vinyloxy-phenyl)-2-(1-methyl-1H-benzoimidazol-2-yl)-acrylonitrile (*VPBA*)

A mixture of 1-methyl-1H benzoimidazol-2-yl)-acetonitrile (**4**) (23 mg, 0.13 mmol) and 4-methoxy-2-vinyloxy-benzaldehyde (**3**) (24 mg, 0.13 mmol) in ethanol (4 mL) were treated with one drop of piperidine at RT. The solution was stirred for 1 h. No starting was left in TLC. The reaction mixture was evaporated. The obtained crude mass was purified by column chromatography on silica, product eluted with 10–15% ethyl acetate in hexane to afford 3-(4-methoxy-2-vinyloxy-phenyl)-2-(1-methyl-1H-benzoimidazol-2-yl)-acrylonitrile(**VPBA**) (20 mg, 44.8%) as yellow solid. ^{1}HNMR (400 MHz, $CDCl_3$): δ (ppm) = 8.39-8.35 (m, 2H), 7.78 (d, *J* = 7.8 Hz, 1H), 7.38-7.30 (m, 3H), 6.75 (d, *J* = 8.8 Hz, 1H), 6.60-6.56 (m, 2H), 4.87 (d, *J* = 13.64 Hz, 1H), 4.58 (d, *J* = 5.76 Hz, 1H), 3.99 (s, 3H), 3.87 (s, 3H). ^{13}C NMR (100 MHz, $CDCl_3$): 164.03, 157.61, 148.34, 146.96, 145.08, 142.46, 136.71, 129.98, 123.58, 122.97, 119.95, 117.32, 115.98, 109.68, 108.89, 102.37, 98.23, 97.37, 55.77, 31.63. MS (ESI): *m*/*z* calc. for $C_{20}H_{17}N_3O_2$: 331.13; found: 332.14 $[M+H]^+$.

2.3.5. Preparation of 7-Methoxy-3-(1-methyl-1H-benzoimidazol-2-yl)-chromen-2-ylideneamine (*5*)

A mixture of 3-(4-methoxy-2-vinyloxy-phenyl)-2-(1-methyl-1H-benzoimidazol-2-yl)-acrylonitrile (**VPBA**) (50 mg, 0.15 mmol) and mercuric chloride (40.7 mg, 0.13 mmol) in acetonitrile (4 mL)/water(1 mL) at RT. The reaction mixture was stirred for 1–2 h. The resultant solid was filtered and dried to afford 7-Methoxy-3-(1-methyl-1H-benzoimidazol-2-yl)-chromen-2-ylideneamine(**5**) (20 mg, 43%) as brown solid. ^{1}HNMR (400 MHz, $CDCl_3$): δ (ppm) = 7.79 (d, *J* = 7.2 Hz, 1H), 7.5 (s, 2H), 7.38 (d, *J* = 7.2, 1H), 7.34-7.28 (m, 3H), 6.73 (dd, *J* = 17.6, and 20.0 Hz, 2H), 3.87 (s, 3H), 3.83 (s, 3H). ^{13}C NMR (100 MHz, $CDCl_3$):163.05, 155.52, 142.8, 136.29, 129.27, 123.11, 122.37, 119.98, 112.27, 111.17, 109.72, 100.64, 55.78, 31.69. MS (ESI): *m*/*z* calc. for $C_{18}H_{15}N_3O_2$: 305.12; found: 306.0 $[M+H]^+$.

3. Results and discussion

To understand the recognition behaviour of **VPBA** and the generated fluorophore, we carried out absorption and emission spectroscopic studies, ^{1}H NMR spectroscopy and computations based on the density functional theory (DFT). Spectroscopic experiments were carried out in aqueous acetonitrile (CH_3CN: H_2O = 2:3 v/v, 10 mM HEPES buffer, pH = 7.4).

3.1. UV–vis and fluorescence spectroscopic studies

In order to confirm the reactivity of different metal ions with probe **VPBA**, and their preferential reactivity toward Hg^{2+} over the other ions has been studied by absorption and fluorescence titrations. The UV–vis absorption spectra of chemosensor **VPBA** in aqueous acetonitrile (CH_3CN:H_2O = 2:3 v/v, 10 mM HEPES buffer, pH = 7.4) were moderately displayed by two absorption bands at 284 and 345 nm, respectively. During the titration, the concentration of probe **VPBA** was kept constant at 10 μM and the mole ratio of Hg^{2+} was varied. Upon addition of Hg^{2+} (0–2 equiv.), the absorption band at 345 nm decreased and a new band at 375 nm appeared (Fig. 1). Instantly with an isosbestic point at 355 nm, which is owing to the loss of vinyl enol ether group and the formation of cyclic compound **5** (Scheme 2).

The fluorescence properties of **VPBA** were investigated in aqueous acetonitrile (CH_3CN:H_2O = 2:3 v/v, 10 mM HEPES buffer, pH = 7.4). As expected, the probe VPBA exhibited very weak emission i.e. almost non-fluorescent (Φ = 0.004) when excited at

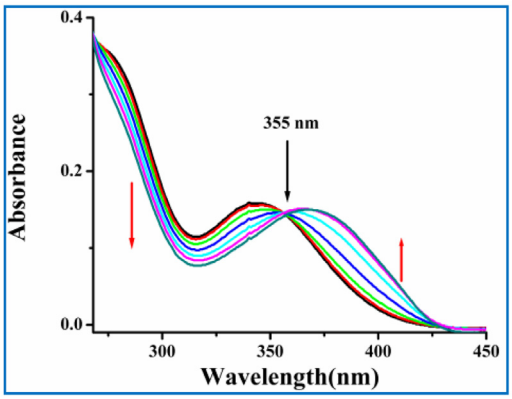

Fig. 1. Absorption spectra of **VPBA** (10 μM) upon addition of increasing concentration of Hg^{+2} (0–2 equiv.) in aqueous acetonitrile ($CH_3CN:H_2O$ = 2:3 v/v, 10 mM HEPES buffer, pH = 7.4). Spectra were recorded after incubation with Hg^{+2} for 10 min at room temperature.

when 2.5 equiv. of Hg^{2+} was added. Spectra were recorded after 10 min of each addition of Hg^{2+} (100 μM) solution.

Thus, the new peak appeared at 455 nm can be recognized to the fluorescence emission of the reaction product. Hence these results indicated that the probe **VPBA** reacted with Hg^{2+} at room temperature to generate iminocoumarin fluorophore **5**. In addition, the fluorescent color of the **VPBA** solution upon interaction with Hg^{2+} changed from colorless to turquoise blue under UV light at 365 nm (see Fig. 2(a) inset), which would allow fluorescence naked eye detection of Hg^{2+}.

3.2. Selectivity in sensing

In order to check whether **VPBA** was selective to only Hg^{2+} or even to the other ions, fluorescence titrations were carried out in the same medium with 16 different metal ions (apart from Hg^{2+}), viz. Al^{3+}, Na^{+}, Co^{2+}, Cr^{3+}, Cu^{2+}, Fe^{2+}, Fe^{3+}, Mg^{2+}, Mn^{2+}, Ni^{2+}, Pb^{2+}, Sn^{4+}, Au^{3+}, Ag^{+}, Ca^{2+}, and Zn^{2+}, and no significant fluorescence enhancement was found in the presence of these ions (Fig. 3a).

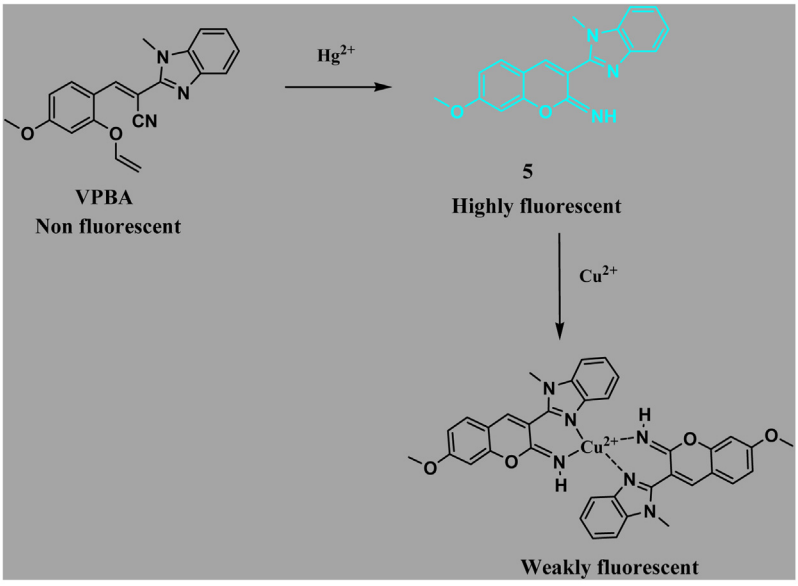

Scheme 2. Sensing of Hg^{2+} and Cu^{2+}.

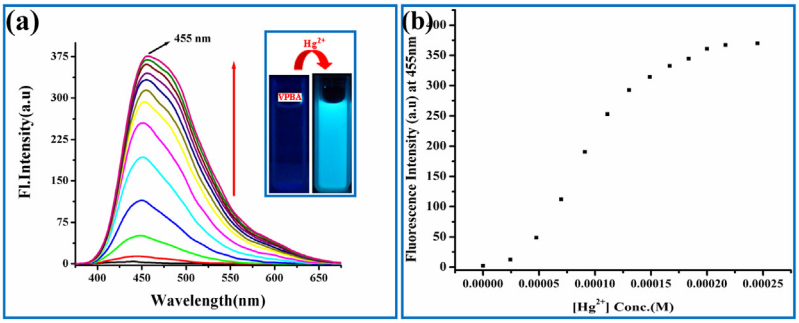

Fig. 2. (a) Fluorescence spectra of VPBA (10 μM) in aqueous acetonitrile ($CH_3CN:H_2O$ = 2:3 v/v, 10 mM HEPES buffer, pH = 7.4) upon addition of different concentration of Hg^{2+} (0- 2.5 equiv.). Each spectrum was recorded after 10 min of addition of Hg^{2+} solution. (b) Change in fluorescence intensity of VPBA with respect to concentration of Hg^{2+}.

355 nm in neutral aqueous solution. Titration of probe **VPBA** (10 μM) with Hg^{2+} resulted in the enhancement of fluorescence intensity at 455 nm as a function of the added Hg^{2+} concentration (Fig. 2) and the enhancement approaches 164-fold at saturation

Much to our delight, the turn-on response of VPBA is highly specific for Hg^{2+}. Fluorescence response of **VPBA** towards Hg^{2+} in presence of the said competing metal ions were also studied and found no significant interference Fig. 3b).

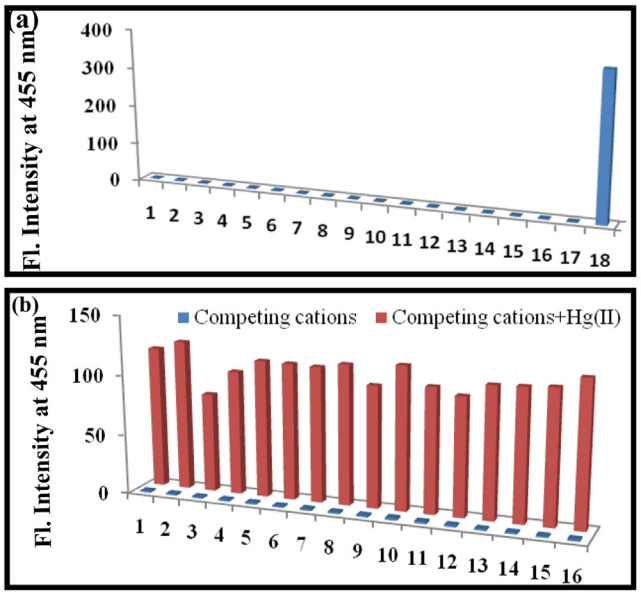

Fig. 3. (a) Fluorescence responses of VPBA (10 mM) to various metal ions, including 2. Al^{3+} 3. Na^{+} 4. Cu^{2+} 5. Cr^{3+} 6. Co^{2+} 7. Fe^{2+} 8. Fe^{3+} 9. Mg^{2+} 10. Mn^{2+} 11. Ni^{2+} 12. Pb^{2+} 13. Sn^{4+} 14. Au^{3+} 15. Ag^{+} 16. Ca^{2+} 17. Zn^{2+} 18. Hg^{2+}. Excitation was at 355 nm and emission was at 455 nm. (b) Fluorescence responses of the receptor VPBA (10 mM) to various metal ions, including 1. Al^{3+} 2. Na^{+} 3. Cu^{2+} 4.Cr^{3+} 5. Co^{2+} 6. Fe^{2+} 7. Fe^{3+} 8. Mg^{2+} 9. Mn^{2+} 10. Ni^{2+} 11.Pb^{2} 12. Sn^{4+} 13.Au^{3+} 14.Ag^{+} 15.Ca^{2+} 16.Zn^{2+} (10 mM). Excitation was at 355 nm and emission was at 455 nm. The blue bars represent the emission intensity of receptor in the presence of other cations. The red bars represent the emission intensity that occurs upon the subsequent addition of Hg^{2+} to the above solutions. (For interpretation of the references to colour in this figure legend, the reader is referred to the web version of this article.).

Minimum detectable concentration was calculated to be 0.39 μM and it has been detected by the fluorescence titrations carried out by keeping the probe to Hg^{2+} mole ratio as 1/1 (Supporting information, Fig. S17). Therefore, **VPBA** can be used for the selective recognition of Hg^{2+} among the 16 different metal ions studied. It should be mentioned that **VPBA** still responds to Hg^{2+} sensitively even in the presence of other relevant competing ions (Fig. 3b).

The fluorescent quantum yield (Φ) of **VPBA** was found to be 0.004 and the isolated intermediate compound 5 show higher (Φ) value of 0.65.

The observed 164-fold increase in the quantum yield of the compound **5**, the presence of water and buffer in the medium of measurements, and the observed low detection limit seem to qualify **VPBA** for sensing Hg^{2+} by switch-on fluorescence.

Under UV light at 365 nm, the solution of **VPBA** is non-fluorescent, whereas in the presence of Hg^{2+} a turquoise blue fluorescent color was observed (Fig. 4) and no such fluorescent color was observed in case of the other metal ions. Thus, Hg^{2+} can easily be differentiated by its fluorescent color change from the other metal ions.

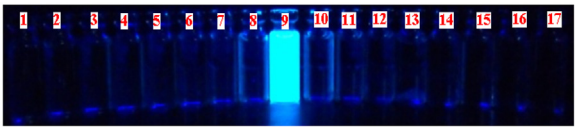

Fig. 4. Change in fluorescence of **VPBA** (10 μM) on addition of various cations sequentially form left to right 1. **VPBA** 2. Al^{3+} 3. Na^{+} 4. Cu^{2+} 5. Cr^{3+} 6. Co^{2+} 7. Fe^{3+} 8. Mn^{2+} 9. Hg^{2+} 10. Ni^{+2} 11. Pb^{+2} 12. Sn^{+4} 13. Au^{+3} 14. Ag^{+1} 15. Ca^{+2} 16.Zn^{+2} 17. Mg^{+2}.

3.3. Selectivity and sensitivity of the generated fluorophore in-situ and isolated compound 5 towards Cu^{2+}

To the solution (**VPBA** + Hg^{2+}) aqueous solution of copper perchlorate was added and a new absorption peak observed, at about 421 nm, and its intensity gradually increased upon the addition of Cu^{2+} (Supporting information, Fig. S15). The color of the solution gradually changed from colorless to light yellowish-green upon the addition Cu^{2+} to probe **VPBA**+ Hg^{2+}. The absorption changed at 375 nm was indicated that relay recognition of these two ions were realized through UV–Vis spectroscopy as well.

Finally, we studied the UV–vis titration of the pure isolated compound **5** with Cu^{2+} ions which exhibited similar type of result to what happened when **VPBA** + Hg^{2+} system was titrated with Cu^{2+}, but the obtained spectra was more prominent and sharp (Supporting information, Fig. S15b). The initial peak at ~375 nm was due to the formation of compound **5**, intensity of which decreased upon gradual addition of Cu^{2+} ions. A bathochromic shift at 439 nm was observed due to ligand-to-metal charge transfer (LMCT). It is important to note that when UV–vis titration with Cu^{2+} was carried out on generated compound **5** in-situ, the UV–vis spectra did not exactly match (especially in higher wavelength region) with that of isolated compound **5**. It may be due to presence of other species e.g. by-product due to loss of vinyl ether, excess Hg^{2+} etc. in the reaction medium of the former.

The in situ generated iminocoumarin **5** has several binding sites exist for coordination, so, the highly fluorescent compound **5** has been used to study for their relay sensing property toward selective cations. Upon the addition of Cu^{2+} (100 μM) to the VPBA + Hg^{2+} solution, fluorescence quenching was indeed observed at 455 nm when excited at 355 nm (Fig. 5).

The total decrease of fluorescence intensity is 64% in the **VPBA**+ Hg^{2+} system when more than 2.0 equivalent of Cu^{2+} was present. The observed fluorescence quench is due to paramagnetic nature of Cu^{2+} and LMCT between the reaction product and Cu^{2+} by coordination, and this behaviour has been further revealed by DFT calculations next section in this paper.

The fast and selective maximum quenching response of 5 toward Cu^{2+} as compared to many cations, including other allied cations viz. Co^{2+}, Cr^{3+}, Cu^{2+}, Fe^{2+}, Fe^{3+}, Mg^{2+}, Mn^{2+}, Ni^{2+}, Pb^{2+}, Sn^{4+}, Ag^{+}, Ca^{2+}, and Zn^{2+} does not show any significant fluorescence change toward any of these cation. Cyclic compound 5 was found to be sensitive to Cu^{2+} even in the presence of other relevant competing ions (Supporting information, Fig. S16). These results clearly demonstrated the resulting **VPBA** + Hg^{2+} solution showed high selectivity for Cu^{2+} in the same media as well. In this way the designed relay recognition of these two ions was achieved with sequence specificity ($Hg^{2+} \rightarrow Cu^{2+}$) via a fluorescence "off-on-off" switching mechanism.

The selectivity was shown on the basis of fluorescence and absorption spectroscopy studies. It was important to note that the above relay recognition of two species ($Hg^{2+} \rightarrow Cu^{2+}$) could be defined as "metal ion → metal ion sequence" with a combination of the chemodosimeter and chemosensor approach that provided a complementary sensing advance to previous bifunctional probes [48,49].

The 1:2 stoichiometry of the **5**-Cu^{2+} was established from the measurements of emission intensity as a function of Cu^{2+} concentration. Plot of relative fluorescence intensity (A-A0) versus [Cu^{2+}]/[Cu^{2+}] + Ligand (**5**) mole ratio showed a clear bend of the curve at 0.65 which suggested that the formation of a 1:2 complex and hence was stoichiometric (Fig. 6).

This stoichiometry in the solution state was also further supported by HR-MS studies. The molecular ion peak appear at *m*/*z* 763.1444, corresponds to the mass of [dimer of **5** + Cu^{2+}] (Supporting information, Fig. S13). The binding constant for the

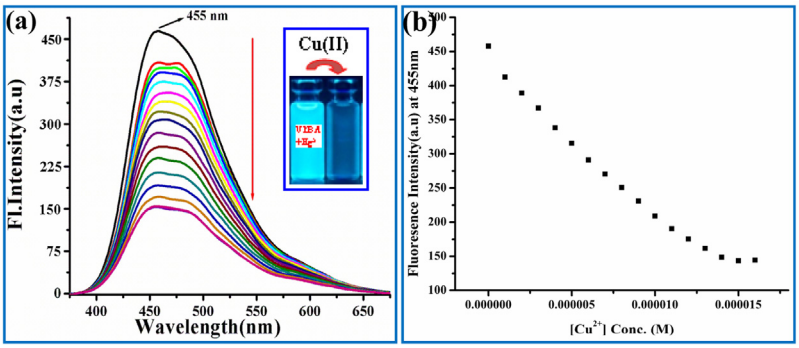

Fig. 5. (a) Fluorescence spectra of **VPBA** (10 μM) + Hg^{2+} (100 μM) upon addition of Cu^{2+} (100 μM) in aqueous acetonitrile ($CH_3CN:H_2O$ = 2:3 v/v, 10 mM HEPES buffer, pH = 7.4). (b) Change in fluorescence intensity of **5** with respect to concentration of Cu^{2+}.

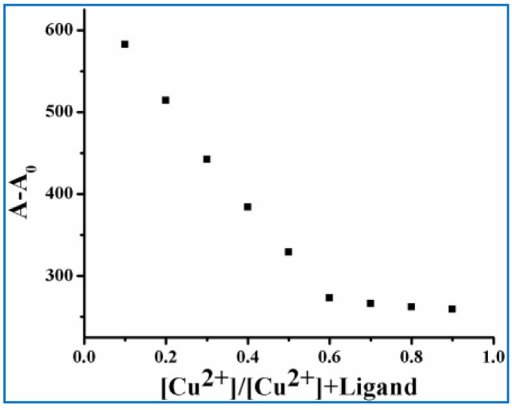

Fig. 6. Job's plot for 5 with Cu^{2+} in aqueous acetonitrile ($CH_3CN:H_2O$ = 2:3 v/v, 10 mM HEPES buffer, pH = 7.4).

formation of **5**-Cu^{2+} complex was calculated on the basis of change of emission at 455 nm by considering 1:2 binding stoichiometry. The binding constant (K) determined by the Benesi–Hildbrand plot experiments was found to be 1.87 × 105 M-1(Supporting information, Fig. S20). The detection limit of **5** for Cu^{2+} ions was found to be 0.74 μM (Supporting information, Fig. S21).

3.4. Reaction mechanism studied by ^{1}H NMR and mass spectral analysis

Furthermore, to confirm the hydrolysis of vinyl enol ether and subsequent cyclization product **5** of probe **VPBA**, we also carried out the ^{1}HNMR and mass studies of probe **VPBA** in the presence of Hg^{2+}. The probe **VPBA** was treated with Hg^{2+}, and the reaction product was isolated by column chromatography over silica gel column and then was subjected to ^{1}H NMR analysis. The partial ^{1}H NMR spectra of **VPBA** and the isolated product **5** are shown in Figure (Supporting information, Fig. S10) The characteristic resonance signal corresponding to the vinyl group of alkenyl protons Ha and H_b from 4.58 to 6.59 ppm completely disappeared and at the same time, the appearance of new peak at 7.59 ppm assigned to the iminocoumarin —NH proton, which indicated that **VPBA** undergoes oxymercuration followed by hydrolysis to generate the compound **5**. To confirm the formation of new molecules, TLC analysis was performed. Interestingly, a fluorescent spot with higher polarity was observed. Moreover, the reaction mechanism was also confirmed by LCMS spectrum analysis, and a peak at *m*/*z* 306.00 corresponding to product **5** was obtained (Supporting information, Fig. S11). For pure probe **VPBA**, a characteristic peak at *m*/*z* = 332.14 was obtained which corresponds to the species [**VPBA** + H]+. Therefore, ^{1}H NMR experiments and mass spectrometry results suggested the validity of the detection mechanism.

3.5. Kinetic study

We studied time-dependent response of probe **VPBA** towards Hg^{2+} (Fig. 7). In this set of experiments, several concentrations of Hg^{2+} ions were tested with a fixed concentration of probe **VPBA** (10 μM). These consequences showed that, upon addition of increasing concentrations of Hg^{2+}, a dramatic increase of emission intensity at 455 nm was observed within 15 min, and the emission signal essentially reached maximum within 26 min. It was observed that 80% of fluorescence enhancing takes place within 15 min of addition of 500 μL of Hg^{2+}(100 μM) at a time. The time dependent fluorescence enhancing indicated that probe **VPBA** was an efficient probe for monitoring the changes in the Hg^{2+} level in living systems.

We then examined the kinetic profiles of the reaction under pseudo-first-order conditions with a large excess of Hg^{2+}

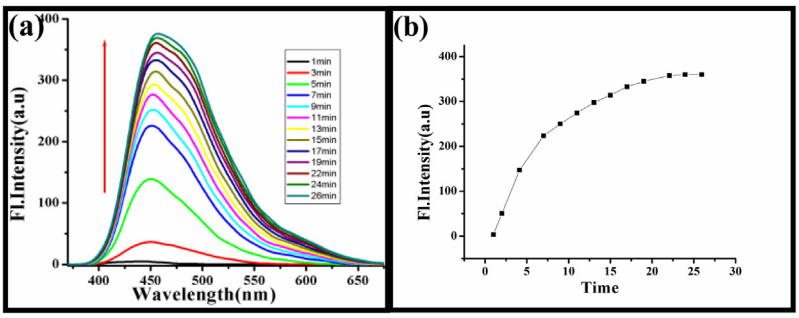

Fig. 7. Time dependent fluorescence spectra (a) and plot (b) of probe VPBA in aqueous acetonitrile ($CH_3CN:H_2O$ = 2:3 v/v, 10 mM HEPES buffer, pH = 7.4) in presence of Hg^{2+}.

(500.0 μM) over probe **VPBA** (10.0 μM) in aqueous acetonitrile ($CH_3CN:H_2O$ = 2:3 v/v, 10 mM HEPES buffer, pH = 7.4) at room temperature. The pseudo-first-order rate constant k/was calculated according to Eq. (1):

$$\ln[(F_{max}-F_t)/F_{max}] = -K^{/}t \quad \ldots \ldots (1)$$

where F_t and F_{max} are the fluorescence intensities at 455 nm at time t and the maximum value obtained after the reaction is complete, respectively, and $k^{/}$is the observed pseudo-first-order rate constant and here it is $k^{/} = 0.02561\ s^{-1}$ (Supporting information, Fig. S18).

Based on the results at different concentrations of Hg^{2+}, the second-order rate constant was calculated to be $3.684\ M^{-1}min^{-1}$ (Supporting information, Fig. S19).

3.6. Effect of pH

Moreover, fluorescence titrations of probe **VPBA** with Hg^{2+} at a wide range of pH values was investigated. In the pH range of 1.0–11.0, VPBA alone was inert i.e. exhibited no variation in the fluorescence intensity. (Supporting information, Fig. S14). Also, the fluorescence responses of the probe **VPBA** toward mercury was also found to be almost pH-independent over pH range of 1–11. So, satisfactory Hg^{2+} −sensing abilities were exhibited in the range of pH from 1.0 to 11.0, indicating that **VPBA** could be used in neutral natural systems, or a mildly acidic or basic environment. This indicates that the probe may be suitable for bio-applications at the physiological pH.

3.7. Theoretical study

To get insight into the optical response of probe **VPBA** and their corresponding cyclization product to Hg^{2+} and Cu^{2+}, we carried out density function theory (DFT) and time-dependent density function theory (TD-DFT) calculations at the B3LYP/6-31G(d) level of the Gaussian 09 program. All element except Cu were assigned 6–31 + G(d) basis set. The geometry optimizations for **VPBA**, cyclic compound 5 and their dimeric Cu-complex were done in a cascade fashion starting from semiempirical PM2 followed by ab initio HF to DFT B3LYP by using various basis sets, viz., PM2 → HF/STO-3G → HF/3-21G → HF/6-31G → B3LYP/6-31G(d,p). For Cu complex, a starting model was generated by taking the DFT optimized **5** and placing the Cu^{2+} ion well in the core of the iminocoumarin N and benzoimidazole N as donors moieties at a non-interacting distance. This model was then optimized initially using HF/3-21G level of calculations, and the output structure from this was taken as input for DFT calculations performed using B3LYP with LANL2DZ relativistic pseudopotentials basis set for Cu^{2+} and 6–31 + G(d,p) for all other atoms in the complex.

The geometry optimization of **VPBA** resulted in the nearly planar conformation at the two sides of C=C i.e.; phenyl and benzoimidazole parts and that can be estimated through the dihedral angles (N13-C7-C19-C18 = 177.1; N12-C7-C19-C20 = −170.4) of the two sides. By contrast, the cyclic product iminocoumarin and benzoimidazole moieties in **5** are essentially non planar, with a dihedral angle of ∼1450, ultimately planarity deviate by 350 due to presence of N—CH_3 group in benzoimidazole part. The spatial distributions and orbital energies of HOMO and LUMO of VPBA and cyclization product 5 were also determined (Fig. 8).

The π electrons distribution on the HOMO and the LUMO of 5 are essentially distributed in the entire iminocoumarin−benzoimidazole backbone. By contrast, in the case of **VPBA**, the π electrons on HOMO is mainly distributed at the benzene ring and benzoimidazole moieties, whereas on the LUMO is mainly located on the electron withdrawing cyano group. This indicates that **VPBA** bears electron transfer from the benzene/benzoimidazole moiety to the cyano group, thus rendering the fluorescence relatively weak (ϕ = 0.004).

By contrast, the nearly complete overlap of electrons on the transition orbitals may induce the strong fluorescence emission for **5** (ϕ = 0.65). Moreover, the HOMO−LUMO energy gap of **5** become smaller relative to that of probe **VPBA**, and hence the ICT character of the **5** is only modest as a result an obvious changes in the absorption spectra observed at 375 nm upon treatment of **VPBA** with Hg^{2+} cations. The energy gaps between HOMO and LUMO in the probe **VPBA** and **5** were 3.83 eV and 3.68 eV respectively (Fig. 8)

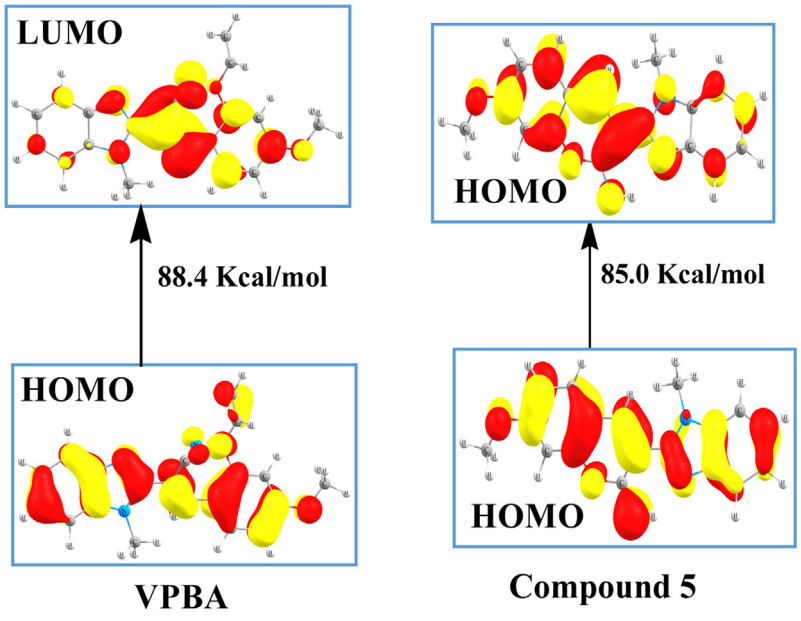

Fig. 8. HOMO-LUMO distribution of **VPBA** and Compound **5.**

As the stiochiometry of the complex formed between Cu^{2+} and **5** was found to be 1:2 based on emission, absorption, and HR-MS studies, so its dimeric Cu-complex structure was optimized. The optimized structure of Cu-complex shows that the copper is bound by two molecules of cyclic compound **5** to satisfy the need for saturated coordination through centro-symmetric four nitrogen atoms (two iminocoumarin nitrogens and two imidazole nitrogens) in the binding core N4 leads to highly regular square planar geometry, and the whole molecular system forms a nearly planar structure. The optimized complex of Cu^{2+} with **5** associated with four bonds (2 × Nimine–Cu and 2 × Nimidazole–Cu) to the central ion with their distances of 1.973 and 1.983 Å respectively (Supporting information, Fig. S24c). Moreover, the HOMO–LUMO energy gap of complex becomes much smaller relative to that of both probe VPBA and cyclization product **5**.

The energy gaps between HOMO and LUMO in the Cu-complex and cyclic compound **5** were 2.42 eV and 3.68 eV respectively (Supporting information, Table S1). The initial peak of compound **5** at 373 nm was due to HOMO to LUMO electronic transition as evident from DFT calculation (Supporting information, Table S1). The π electrons on the HOMO of Cu-complex is mainly located on the iminocoumarin and benzoimidazole framework, but the LUMO is mostly positioned at the center of the guest Cu^{2+} ion, which indicated a strong ligand-to-metal charge transfer (LMCT) process (Fig. 9). Thus, **5** acts as a quenching fluorescent probe toward Cu^{2+} ion. The origin of the bathochromic shift (λ_{max} 372 nm → 439 nm) in the absorption spectra of the Cu-complex compared with that for **5** is attributed to LMCT between the **5** and Cu^{2+} by effective coordination.

In addition, we also performed time-dependent density function theory (TD-DFT) calculations to explain the electronic properties of these complexes in their ground and excited states. The vertical transitions i.e, the calculated λ_{max}, main orbital transition, and oscillator strength (f) are listed in Table S1 in the Supporting information. The vertical transitions calculated by TD-DFT were compared with the experimental UV–Vis spectra of **VPBA**, **5** and Cu-complex and were found to have good agreement with the experimental data.

Table 1
Determination of Hg2+ from natural water sample.

Sample	Added Hg^{2+}(μM)	Found Hg^{2+}(μM)	Recover (%)	RSD (%)
River Water.	5.0	5.12	102.4	1.62
	10.0	10.23	102.3	1.78
Pond Water	5.0	4.87	97.4	1.82
	10.0	9.92	99.2	0.89
Tap Water	5.0	5.20	104.0	1.70
	10.0	10.19	101.9	1.12

3.8. Practical application of *VPBA*

The practicability of the probe **VPBA** for detecting Hg^{2+} in real samples was explored by analysis of natural water. To do this, we collected different water samples (river water, pond water and tap water) and detect Hg^{2+} using our probe **VPBA**. The water samples were spiked with standard solutions containing different concentrations of Hg^{2+}.

The results are displayed in Table 1. For the three samples, similar results were obtained and good recovery rates range from 97.4 to 104.0% was found. The relative standard deviation (RSD) of three measurements was less than 1.82%. These results suggested that the probe VBPA was suitable for detection of Hg2+ in real water sample.

3.8.1. Cytotoxicity assay

To demonstrate the practical application of the probe (**VPBA**) we have done the live cell imaging to detect even trace amount of Hg^{2+}. Vero cells were used to detect Hg^{2+} ions in live cells. In this context, we have also detected trace amount of Cu^{2+} in live cells by using compound **5**. However, to materialize this objective we have probed the cytotoxic effect of **VPBA**, Hg^{2+}, Compound **5**, Cu^{2+} and 5-Cu^{2+} on live cells. We have performed MTT assay, which is based on mitochondrial dehydrogenase activity of viable cells to study cytotoxicity of above mentioned compounds at varying concentrations mentioned in method section (Supporting information, Fig. S22 and S23). The experiment shows that probe **VPBA** and

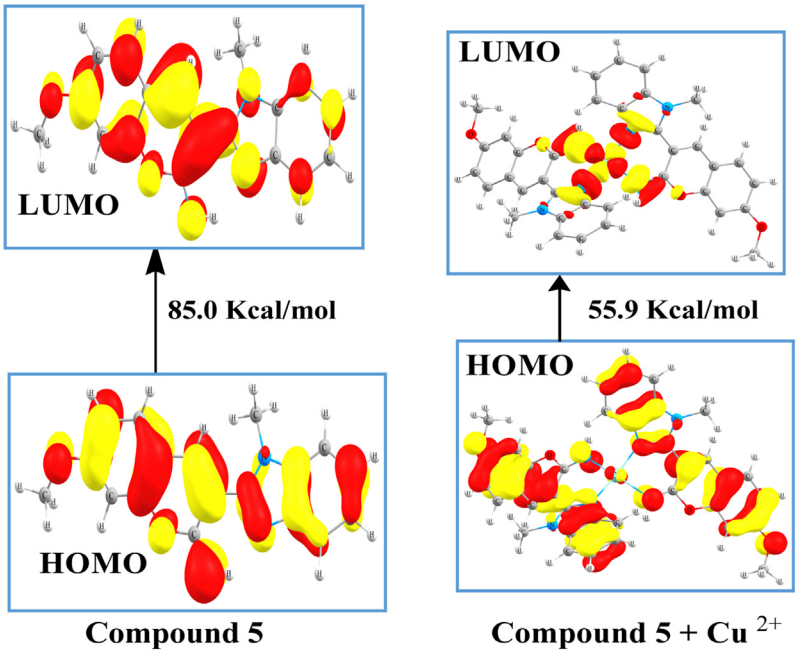

Fig. 9. HOMO-LUMO distribution of Compound **5** and **5** + Cu^{2+}.

compound **5** did not exert any significant effect on cell viability; however the Hg^{2+} and Cu^{2+} ions have dose dependent adverse effect when cells were treated with varying concentrations of $Hg^{2+}$and Cu^{2+}. The metal-probe complex has the significant adverse effect on cell viability beyond 75 μM. The effect is more pronounced in higher concentration and has showed an adverse cytotoxic effect in a dose-dependent manner. The viability of vero cells is not influenced by the solvent (DMSO).

*3.8.2. Application of **VPBA** in live cell imaging*

The results obtained in the in vitro cytotoxic assay has revealed that, in order to pursue fluorescence imaging studies of metal-probe complex in live cells, it would be cautious to choose a working concentration of 10–20 μM for probe compound. So, to assess the effectiveness of compound, first cells are treated with **VPBA**, followed by 20 μM Hg^{2+} for 1 h. Fluorescent microscopic studies has revealed a lack of fluorescence in vero cells when treated with Hg^{2+} (Fig. 10a) and the probe alone (Fig. 10c). When the cells are treated with the probe **VPBA** in presence of Hg^{2+}, a striking Green fluorescence is observed inside the cells, which indicates the formation of compound **5**, as observed earlier in solution studies (Fig. 10e&f). Consequently, quenching of fluorescence intensity was observed after addition of Cu^{2+} ((Fig. 10g&h).

The fluorescent microscopic studies suggested that probe **VPBA** could eagerly cross the membrane barrier of the vero cells, and quickly sense intracellular Hg^{2+} and Cu^{2+} in very low concentration. Most importantly, bright field images of treated cells did not expose any gross morphological changes, which suggested that vero cells are viable. These results open up the path for future in vivo biomedical applications of this sensor.

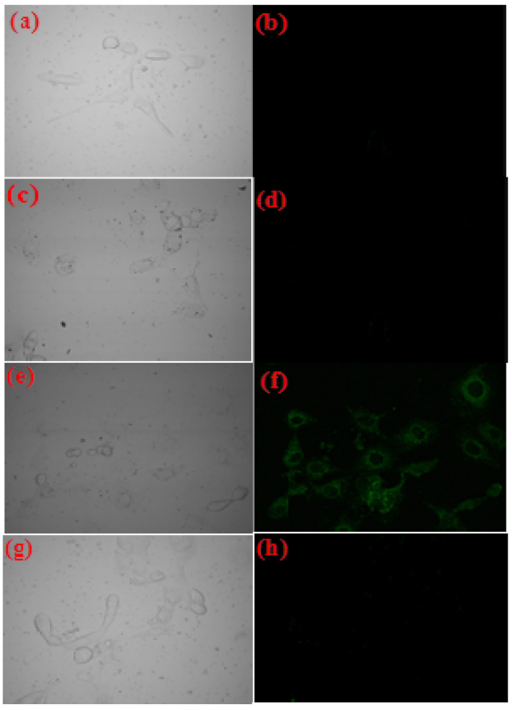

Fig. 10. Fluorescence images of probe in vero cell (a) Bright field image of the cells stained with Hg^{2+} at 2.0×10^{-5}M concentration (b) Fluorescence images of the cells treated with Hg^{2+} at 2.0×10^{-5}M concentration (c) Bright field image of the cells stained with probe **VPBA** at concentration 1.0×10^{-6}M (in green filter) (d) Fluorescence images of the cells treated with probe **VPBA** (e) Bright field image of the cells stained with probe **VPBA** + Hg^{2+}. (f) Fluorescence images of the cells treated with probe **VPBA** + Hg^{2+}(in green filter). (g) Bright field image of the cells stained with probe **5** + Cu^{2+}. (h) Fluorescence images of the cells treated with **5** + Cu^{2+}. (For interpretation of the references to colour in this figure legend, the reader is referred to the web version of this article.).

4. Conclusions

In conclusion we may state that our probe **VPBA** is an efficient, selective and sensitive probe that successfully demonstrates both chemodosimetry and traditional co-ordination based sensing for two different analytes with sequence specificity ($Hg^{2+} \rightarrow Cu^{2+}$) via a fluorescence "off-on-off" mechanism. The well-known hydrolysis reaction of vinyl enol ether by mercury is exploited in the chemodosimetric approach and the sensing response was quantified through the intensity of turn-on fluorescence response. This hydrolysis reaction led to formation of highly fluorescent iminocoumarin species which participated in 1:2 co-ordination with Cu^{2+}. Especially, iminocoumarin **5** is also potentially useful for quantitative determination of Cu^{2+} by absorption and fluorescence titration in aqueous acetonitrile ($CH_3CN:H_2O = 2:3$ v/v, 10 mM HEPES buffer, pH = 7.4). The spectral changes have been corroborated by DFT studies as well as mass and ^1H NMR spectra. Further, the presence of the coumarin moiety makes this probe an ideal candidate for applications in intracellular imaging studies which has also been successfully demonstrated in this work.

Acknowledgment

We acknowledge DAE-BRNS, India [Project No. 36(1)/14/12/2016-BRNS/36012] for financial support.

Appendix A. Supplementary data

Supplementary data associated with this article can be found, in the online version, at http://dx.doi.org/10.1016/j.jphotochem.2017.04.011.

References

[1] J.J. Lavigne, E.V. Anslyn, Sensing a paradigm shift in the field of molecular recognition: from selective to differential receptors, Angew. Chem. Int. Ed. 40 (2001) 3118–3130.
[2] N. Singh, R.C. Mulrooney, N. Kaur, J.F. Callan, A nanoparticle based chromogenic chemosensor for the simultaneous detection of multiple analytes, Chem. Commun. 40 (2008) 4900–4902.
[3] R. Satapathy, Y.H. Wu, H.C. Lin, Novel thieno-imidazole based probe for colorimetric detection of $Hg^{2+}$and fluorescence turn-on response of Zn^{2+}, Org. Lett. 14 (2012) 2564–2567.
[4] R. Guliyev, S. Ozturk, E. Sahin, E.U. Akkaya, Expanded bodipy dyes: anion sensing using a Bodipy analog with an additional difluoroboron bridge, Org. Lett. 14 (2012) 1528–1531.
[5] M. Schmittel, S. Qinghai, A lab-on-a-molecule for anions in aqueous solution: using Kolbe electrolysis and radicalmethylation at iridium for sensing, Chem. Commun. 48 (2012) 2707–2709.
[6] V. Bhalla, R. Kumar, M. Kumar, A. Dhir, Bifunctional fluorescent thiacalix[4] arene based chemosensor for Cu2+ and F- ions, Tetrahedron 63 (2007) 11153–11159.
[7] Z. Xu, S. Kim, H.N. Kim, S.J. Han, C. Lee, J.S. Kim, X. Qian, J. Yoon, A naphthalimide–calixarene as a two-faced and highly selective fluorescent chemosensor for Cu^{2+} or F^-, Tetrahedron Lett. 48 (2007) 9151–9154.
[8] E.J. Song, J. Kang, G.R. You, G.J. Park, Y. Kim, S.J. Kim, C. Kim, R.G. Harrison, A single molecule that acts as a fluorescence sensor for zinc and cadmium and a colorimetric sensor for cobalt, Dalton Trans. 42 (2013) 15514–15520.
[9] L. Qu, C. Yin, F. Huo, J. Chao, Y. Zhang, F. Cheng, A pyridoxal-based dual chemosensor for visual detection of copper ion and ratiometric fluorescent detection of zinc ion, Sens. Actuators B 191 (2014) 158–164.
[10] M. Wang, F. Yan, Y. Zou, L. Chen, N. Yang, X. Zhou, Recognition of Cu^{2+} and Hg^{2+} in physiological conditions by a new rhodamine based dual channel fluorescent probe, Sens. Actuators B 192 (2014) 512–521.
[11] A.K. Mahapatra, R. Maji, K. Maiti, S. Mondal, S.S. Ali, S.K. Manna, P. Sahoo, Carbazole-driven ratiometric fluorescence turn on for dual ion recognition of Zn2+ and Hg2+ by thiophene-pyridyl conjugate in HEPES buffer medium: spectroscopy, computational, Microsc. Cell. Stud. Supramolecular Chem. (2016), doi:http://dx.doi.org/10.1080/10610278.2016.1202412.
[12] L. Magos, Physiology and toxicology of mercury, Met. Ions Biol. Syst. 34 (1997) 321–370.
[13] M.F. Wolfe, S. Schwarzbach, R.A. Sulaiman, The Effects of mercury on wildlife: a comprehensive review: environmental toxicology and chemistry, Environ. Toxicol. Chem. 17 (1998) 146–160.

[14] P. Grandjean, P. Weihe, R.F. White, F. Debes, Cognitive performance of children prenatally exposed to safe levels of methylmercury, Environ. Res. 77 (1998) 165–172.
[15] S.H. Choi, K. Pang, K. Kim, D.G. Churchill, Cu^{2+} colorimetric sensing and fluorescence enhancement and Hg^{2+}Fluorescence diminution in scorpionate-like tetrathienyl-substituted boron-dipyrrins, Inorg. Chem. 46 (2007) 10564–10577.
[16] A. Renzoni, F. Zinoand, E. Franchi, Mercury levels along the food chain and risk for exposed populations, Environ. Res. 77 (1998) 68–72.
[17] Mercury Update: Impact on Fish Advisories, EPA Fact Sheet EPA- 823-F-01-011, EPA, Office of Water, Washington DC, 2001.
[18] R. Von Burg, M.R. Greenwood, Metals and Their Compounds in the Environment, in: E. Merian (Ed.), VCH, Weinheim, 1991, pp. 1045–1088.
[19] M. Harada, Minamata disease: methylmercury poisoning in Japan caused by environmental pollution, Crit. Rev. Toxicol. 25 (1995) 1–24.
[20] R. Von Burg, Inorganic mercury, J. Appl. Toxicol. 15 (1995) 483–493.
[21] T.W. Clarkson, L. Magos, G.J. Myers, The toxicology of mercury—current exposures and clinical manifestations, N. Engl. J. Med. 349 (2003) 1731–1737.
[22] A. Mathie, G.L. Sutton, C.E. Clarke, E.L. Veale, Zinc and copper: pharmacological probes and endogenous modulators of neuronal excitability, Pharm. Ther. 111 (2006) 567–583.
[23] P.C. Bull, G.R. Thomas, J.M. Rommens, J.R. Forbes, D.W. Cox, The Wilson disease gene is a putative copper transporting P-type ATPase similar to the Menkes gene, Nat. Genet. 5 (1993) 327–373.
[24] J.S. Valentine, P.J. Hart, Misfolded CuZnSOD and amyotrophic lateral sclerosis, Proc. Natl. Acad. Sci. U.S.A. 100 (2003) 3617.
[25] C. Vulpe, B. Levinson, S. Whitney, S. Packman, J. Gitschier, Isolation of a candidate gene for Menkes disease and evidence that it encodes a copper-transporting ATPase, Nat. Genet. 3 (1993) 7–13.
[26] L. Zhu, J. Qin, C. Yang, New metal-coordination-inhibited charge transfer emission for terfluorenes: highly sensitive and selective detection for Hg2+ with ratiometric "turn-on" fluorescence response, Chem. Commun. 46 (2010) 8755–8757.
[27] F. Song, S. Watanabe, P.E. Floreancig, K. Koide, Oxidation-resistant fluorogenic probe for mercury based on alkyne oxymercuration, J. Am. Chem. Soc. 130 (2008) 16460–16461.
[28] S. Ando, K. Koide, Development and applications of fluorogenic probes for Mercury(II) based on vinyl ether oxymercuration, J. Am. Chem. Soc. 133 (2011) 2556–2566.
[29] M. Santra, B. Roy, K.H. Ahn, A "Reactive" ratiometric fluorescent probe for mercury species, Org. Lett. 13 (2011) 3422–3425.
[30] Y. Chen, C. Yang, Z. Yu, B. Chen, Y. Han, A highly sensitive hemicyanine-based fluorescent chemodosimeter for mercury ions in aqueous solution and living cells, RSC Adv. 5 (2015) 82531–82534.
[31] Y. Han, C. Yang, K. Wu, Y. Chen, B. Zhou, M. Xia, A facile naphthalene-based fluorescent chemodosimeter for mercury ions in aqueous solution, RSC Adv. 5 (2015) 16723–16726.
[32] K.P. Carter, A.M. Young, A.E. Palmer, Fluorescent sensors for measuring metal ions in living systems, Chem. Rev. 114 (2014) 4564–4601.
[33] E.M. Nolan, S.J. Lippard, Tools and tactics for the optical detection of mercuric ion, Chem. Rev. 108 (2008) 3443–3480.
[34] X. Chen, T. Pradhan, F. Wang, J.S. Kim, J. Yoon, Fluorescent chemosensors based on spiroring-opening of xanthenes and related derivatives, Chem. Rev. 112 (2012) 1910–1956.
[35] Z. Guo, S. Park, J. Yoon, I. Shin, Recent progress in the development of near-infrared fluorescent probes for bioimaging applications, Chem Soc. Rev. 43 (2014) 16–29.
[36] L. Yuan, W. Lin, K. Zheng, L. He, W. Huang, Far-red to near infrared analyte-responsive fluorescent probes based on organic fluorophore platforms for fluorescence imaging, Chem. Soc. Rev. 42 (2013) 622–661.
[37] J. Fan, M. Hu, P. Zhan, X. Peng, Energy transfer cassettes based on organic fluorophores: construction and applications in ratiometric sensing, Chem. Soc. Rev. 42 (2013) 29–43.
[38] J. Du, M. Hu, J. Fan, X. Peng, Fluorescent chemodosimeters using mild chemical events for the detection of small anions and cations in biological and environmental media, Chem. Soc. Rev. 41 (2012) 4511–4535.
[39] N. Thakur, S.A. Kumar, K.S.A. Kumar, A.K. Pandey, S.D. Kumar, A.V.R. Reddy, Development of a visual optode sensor for onsite determination of Hg(II), Sens. Actuators B 211 (2015) 346–353.
[40] N. Kumari, N. Dey, S. Jha, S. Bhattachary, Ratiometric, reversible, and parts per billion level detection of multiple toxic transition metal ions using a single probe in micellar media, ACS Appl. Mater. Interfaces 5 (2013) 2438–2445.
[41] Y. Zhou, C.-Y. Zhu, X.-S. Gao, X.-Y. You, C. Yao, Hg^{2+}-Selective ratiometric and off-on chemosensor based on the azadiene-pyrene derivative, Org. Lett. 12 (2010) 2566–2569.
[42] M. Vedamalai, S. Wu, A BODIPY-based highly selective fluorescent chemosensor for Hg^{2+} ions and its application in living cell imaging, Eur. J. Org. Chem. 6 (2012) 1158–1163.
[43] R. Maji, A.K. Mahapatra, K. Maiti, S. Mondal, S.S. Ali, P. Sahoo, S. Mandal, M.R. Uddin, A highly sensitive fluorescent probe for detection of hydrazine in gas and solution phases based on the Gabriel mechanism and its bioimaging, RSC Adv. 6 (2016) 70855–70862.
[44] A.K. Mahapatra, R. Maji, K. Maiti, S.K. Manna, S. Mondal, S.S. Ali, S. Manna, P. Sahoo, S. Mandal, M.R. Uddin, D. Mandal, A BODIPY/pyrene-based chemodosimetric fluorescent chemosensor for selective sensing of hydrazine in the gas and aqueous solution state and its imaging in living cells, RSC Adv. 5 (2015) 58228–58236.
[45] A.K. Mahapatra, K. Maiti, S.K. Manna, R. Maji, S. Mondal, C.D. Mukhopadhyay, P. Sahoo, D. Mandal, A cyclization-induced emission enhancement (CIEE)-based ratiometric fluorogenic and chromogenic probe for the facile detection of a nerve agent simulant DCP, Chem. Commun. 51 (2015) 9729–9732.
[46] A.K. Mahapatra, P. Karmakar, J. Roy, S. Manna, K. Maiti, P. Sahoo, D. Mandal, Colorimetric and ratiometric fluorescent chemosensor for fluoride ions based on phenanthroimidazole (PI): spectroscopic, NMR and density functional studies, RSC Adv. 5 (2015) 37935–37942.
[47] A.K. Mahapatra, K. Maiti, R. Maji, S.K. Manna, S. Mondal, S.S. Ali, S. Manna, Ratiometric fluorescent and chromogenic chemodosimeter for cyanide detection in water and its application in bioimaging, RSC Adv. 5 (2015) 24274–24280.
[48] Y. Xu, L. Xiao, S. Sun, Z. Pei, Y. Pei, Y. Pang, Switchable and selective detection of Zn^{2+} or Cd^{2+}in living cells based on 3′-*O*-substituted arrangement of benzoxazole-derived fluorescent probes, Chem. Commun. 50 (2014) 7514–7516.
[49] Z. Liu, W. He, M. Pei, G. Zhang, A fluorescent sensor with a detection level of pM for Cd^{2+} and nM for Cu^{2+} based on different mechanisms, Chem. Commun. 51 (2015) 14227–14230.